View metadata, citation and similar papers at core.ac.uk

brought to you by CORE

provided by Universiti Teknologi Malaysia Institutional Repository

Mechanical Systems and Signal Processing 98 (2018) 157–172

Contents lists available at ScienceDirect

Mechanical Systems and Signal Processing

journal homepage: www.elsevier.com/locate/ymssp

Adaptive output-based command shaping for sway control of a 3D overhead crane with payload hoisting and wind disturbance

Auwalu M. Abdullahi [a], Z. Mohamed [a,*], H. Selamat [a], Hemanshu R. Pota [b], M.S. Zainal Abidin [a], F.S. Ismail [a], A. Haruna [a]

[a] Faculty of Electrical Engineering, Universiti Teknologi Malaysia, 81310 UTM Johor Bahru, Johor, Malaysia
[b] School of Engineering and Information Technology, The University of New South Wales, Australian Defence Force Academy, Canberra, ACT 2600, Australia

ARTICLE INFO

Article history:
Received 19 December 2016
Received in revised form 21 April 2017
Accepted 24 April 2017
Available online 6 May 2017

Keywords:
Adaptive command shaping
Input shaping
Overhead crane
Payload hoisting
Sway control
Wind disturbance

ABSTRACT

Payload hoisting and wind disturbance during crane operations are among the challenging factors that affect a payload sway and thus, affect the crane's performance. This paper proposes a new online adaptive output-based command shaping (AOCS) technique for an effective payload sway reduction of an overhead crane under the influence of those effects. This technique enhances the previously developed output-based command shaping (OCS) which was effective only for a fixed system and without external disturbances. Unlike the conventional input shaping design technique which requires the system's natural frequency and damping ratio, the proposed technique is designed by using the output signal and thus, an online adaptive algorithm can be formulated. To test the effectiveness of the AOCS, experiments are carried out using a laboratory overhead crane with a payload hoisting in the presence of wind, and with different payloads. The superiority of the method is confirmed by 82% and 29% reductions in the overall sway and the maximum transient sway respectively, when compared to the OCS, and two robust input shapers namely Zero Vibration Derivative-Derivative and Extra-Insensitive shapers. Furthermore, the method demonstrates a uniform crane's performance under all conditions. It is envisaged that the proposed method can be very useful in designing an effective controller for a crane system with an unknown payload and under the influence of external disturbances.

© 2017 Elsevier Ltd. All rights reserved.

1. Introduction

An overhead crane system is widely used in industries and seaports to transport large and heavy containers/payloads. In order to increase productivity, the crane is expected to transport the payload as fast as possible to its destination. However, the crane acceleration and deceleration generates payload sways especially during loading and unloading operations [1,2]. In practice, payload hoisting is a common operation and this action also generates unwanted crane motions such as load bouncing, twisting and swinging. Furthermore, an external disturbance such as wind is another factor that considerably affects the payload sway. All these unwanted motions affect a payload's positioning precision and thus decrease an overall crane's performance and reduces the overall productivity [3]. These sways may also result in accidents and damages to the neighbouring facilities. As precise payload positioning and sways control of a crane is difficult especially with hoisting and under the influence of external disturbances, the crane operation is not automatic and continuously requires an operator to monitor

* Corresponding author.
E-mail address: zahar@fke.utm.my (Z. Mohamed).

http://dx.doi.org/10.1016/j.ymssp.2017.04.034
0888-3270/© 2017 Elsevier Ltd. All rights reserved.

the crane during operation [4]. An effective control is required to achieve safety and effectiveness of crane operations [5]. Development of an efficient controller for reduction of payload sway is desirable as this will reduce complexity of designing a controller for both position and sway control. Several investigations and control approaches have previously been investigated to handle the problems, and they can be classified into feedforward and feedback control approaches [6].

A feedback control uses the system's states in order to reduce the effect of the unwanted oscillation and also for tracking and regulation control [7]. Recently, an error tracking control of an overhead crane [8] and an adaptive error tracking control to handle external disturbances and parametric uncertainties of an overhead crane [9] were proposed. In addition, a flatness-based finite-time [10] and a nonlinear output feedback control [11] were also investigated for anti-swing control of crane systems.

On the other hand, a feedforward control alters the command input signal to cancel the system's oscillation. A number of feedforward controls have been developed using Finite Impulse Response (FIR) filters for vibration control of crane systems. These include a FIR filter for a rotary crane [12], and a boom crane [13]. Another form of feedforward control is a command smoothing approach where system vibrations are suppressed by smoothing the original command [14]. The smoother was designed by estimating the system's natural frequency and the damping ratio. In [15,16], the command smoothing was used for sway control of a bridge crane with a double-pendulum and a distributed payload mass. Recently, a hybrid control with command smoothing and a wind-rejection command was proposed to suppress operator-induced sway and to reject wind disturbance of a bridge crane with a distributed-mass payload [17].

One of the most popular feedforward control methods is an input shaping approach. By using this method, system vibration is reduced by convolving a command input signal with a sequence of impulses that are designed based upon the natural frequency and the damping ratio of a system. The earliest input shaping approach was introduced in [18]. Since then, several modified input shaping techniques have been presented and applied to various crane systems. These include Zero Vibration (ZV) and Zero Vibration Derivative (ZVD) shapers [19,20], positive and negative input shapers [21], finite-state input shaping [22], extra intensive shaper [23], an input shaping designed with a distributed delay [24] and an improved input shaper for a nonlinear crane with friction [25]. Recently, a shaper based on a system output was designed and implemented on a laboratory 3D crane system [26], and showed a promising result for reducing payload sways. However, most of these input shaping methods were designed for systems with fixed parameters and time-invariant. Therefore, these input shapers were not robust when applied to systems with uncertainties or time-variant in which the natural frequencies and damping ratios of systems change during payload hoisting, payload variation and in the presence of wind.

In order to minimise the effects of the payload hoisting and payload variation, several modified and adaptive input shapers have been proposed. These include an adaptive input shaping for 3D overhead cranes [27], an adaptive input shaping for an overhead crane with hoisting [28], an adaptive algorithm input shaping for variable mass and cable lengths [29], and a modified adaptive input shaping [30]. Furthermore, an input shaper designed by using an average travel hoisting length (ATL) technique was also proposed [31]. Some control efforts were also investigated to control the wind effects on crane systems [16,32,33], in which the controllers were developed based on feedback sensors. Therefore, most of the time, this process gave unavoidable delay in updating the system parameters to reject the wind effect. In addition, the control circuit was complex and expensive.

This paper proposes a new online adaptive output-based command shaping (AOCS) technique for control of an overhead crane with hoisting and in the presence of wind disturbance. The proposed controller provides a significant payload sway reduction and a uniform performance under all conditions. The AOCS is designed to enhance the performance of the previously developed Output-Based Command Shaping (OCS) [26,34], which was effective only for fixed systems and without external disturbance. Using the proposed algorithm, the parameters of the AOCS are adapted to the changes in the cable length and to the effect of wind for different payload weights. Experiments on a laboratory 3D overhead crane are carried out with a payload hoisting operation between 0.22 m and 0.72 m, which corresponds to a decrement in the natural frequency and damping ratio of the system by 41% and 54%, respectively. Moreover, cases with simultaneous hoisting and wind disturbance of 0.3 N applied to payloads of 0.5 kg and 1 kg are also investigated. The robustness and performance of the proposed AOCS is verified by comparing with the experimental results using the OCS, zero vibration derivative-derivative (ZVDD) and extra-insensitive (EI) shapers designed based on the ATL approach. Their performances were assessed in terms of the level of reductions of the transient and residual sways, and the overall sway during hoisting and with the wind.

2. A 3D overhead crane

This section describes the 3D overhead crane used in this study as shown in Fig. 1. The development of a nonlinear model of the crane system is also given. The crane system transfers a load from a particular point to any reference location in a three dimensional space. The length, height and width of the crane are 1.0 m each. The system hardware consists of three main components: a cart, a rail, and a pendulum. The crane has five incremental encoders in order to measure the position of the trolley in both of the X and Y directions, the position of payload in the Z direction, and the payload sway in both of the X and Y directions. Furthermore, an interface card is used in order to transmit all of the experimental data on-line to a computer. In this work, a wind blower serves as the source of the external wind disturbance applied in the direction of the payload sway. The wind speed was measured by using an anemometer and converted into an equivalent wind force.

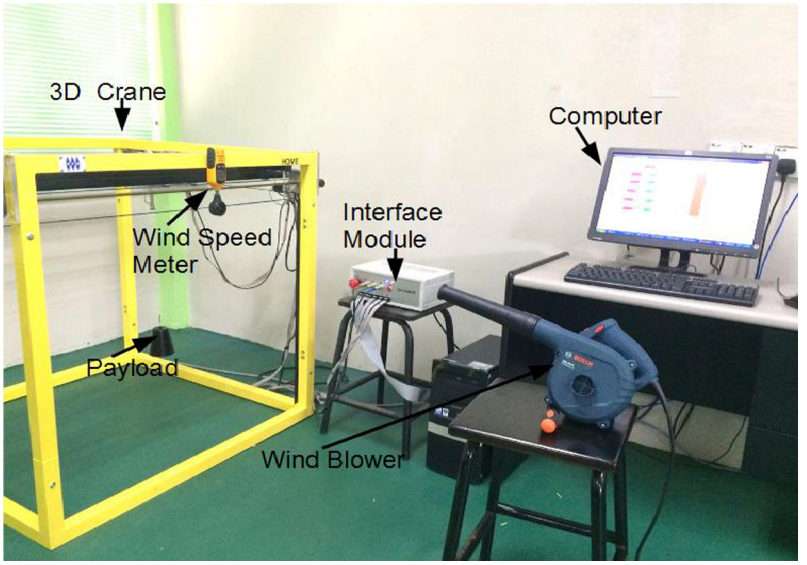

Fig. 1. A laboratory 3D overhead crane.

The mathematical model was obtained by using the Lagrange method based upon the given characteristics of the crane by the manufacturer and the study in [1]. A schematic diagram of the 3D crane system is shown in Fig. 2 with *XYZ* as the coordinate system. α represents the angle of the lift-line with the *Y* axis, and β represents the angle between the negative part of the *Z* axis and the projection of the payload cable onto the *XZ* plane. F_x and F_y are the forces driving the crane in *X* and *Y* directions respectively. F_z is the force lifting the payload and f_x, f_y and f_z are the corresponding viscous damping coefficients on *X*, *Y* and *Z* directions respectively. m_p, m_t and m_r are the payload mass, the trolley mass (including the gear box, the encoders and the DC motor) and the moving rail, respectively, and l represents the length of the cable. With the wind disturbance force, F_d, the equations of motion of the crane are obtained as derived in [1] as

$$\begin{aligned}&(m_t + m_r + m_p)\ddot{x} + m_p l\ddot{\beta}\cos\beta\cos\alpha - m_p l\ddot{\alpha}\sin\beta\sin\alpha + m_p\ddot{l}\sin\beta\cos\alpha + 2m_p\dot{l}\dot{\beta}\cos\beta\cos\alpha - 2m_p\dot{l}\dot{\alpha}\sin\beta\sin\alpha\\&\quad - m_p l\dot{\beta}^2\sin\beta\cos\alpha - m_p l\dot{\alpha}^2\sin\beta\cos\alpha - 2m_p l\dot{\beta}\dot{\alpha}\cos\beta\sin\alpha\\&\quad = F_x - f_x\dot{x}.\end{aligned} \tag{1}$$

$$(m_r + m_p)\ddot{y} + m_p l\ddot{\alpha}\cos\alpha + m_p l\sin\alpha + 2m_p\dot{l}\dot{\alpha}\cos\alpha - m_p l\dot{\alpha}^2\sin\alpha = F_y - f_y\dot{y} \tag{2}$$

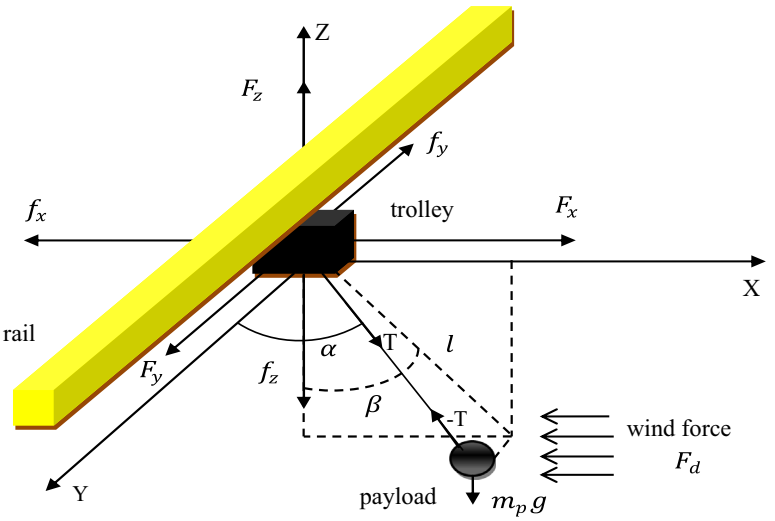

Fig. 2. Schematic diagram and forces.

Table 1
System parameters.

Variables	Values
Mass of payload, m_p	1 kg, 0.5 kg
Mass of trolley, m_t	1.155 kg
Mass of moving rail, m_r	2.2 kg
Hoisting cable length, l	0.22–0.72 m
Gravitational constant, g	9.8 m/s^2
Viscous damping coefficients, f_x, f_y, f_z	100, 82, 75 Ns/m

$$m_p l^2 \ddot{\beta} \cos^2\alpha + m_p l\ddot{x} \cos\beta \cos\alpha + 2m_p l\dot{l}\dot{\beta} \cos^2\alpha + m_p gl \sin\beta \cos\alpha - 2m_p l^2 \dot{\beta}\dot{\alpha} \sin\alpha \cos\alpha = F_{d\beta} \tag{3}$$

$$m_p l^2 \ddot{\alpha} + m_p l\ddot{y} \cos\alpha + m_p gl \sin\alpha \cos\beta - m_p l\ddot{x} \sin\beta \sin\alpha + m_p l^2 \dot{\beta}^2 \sin\alpha \cos\alpha + 2m_p l\dot{l}\dot{\alpha} = F_{d\alpha} \tag{4}$$

$$m_p \ddot{l} + m_p \ddot{x} \sin\beta \cos\alpha + m_p \ddot{y} \sin\alpha - m_p l\dot{\beta}^2 \cos^2\alpha - m_p l\dot{\alpha}^2 - m_p g \cos\alpha \cos\beta = F_z - f_z \dot{l} \tag{5}$$

where x and y represent the trolley and rail positions respectively and g is the gravitational acceleration. The dots represent the velocity and acceleration of the respective variables. $F_{d\beta}$ and $F_{d\alpha}$ are the wind forces acting in the X and Y directions respectively. Table 1 shows the system's parameters which corresponds to the laboratory 3D overhead crane.

3. Control schemes

This section presents the formulations of the proposed AOCS control technique for a payload sway reduction of the crane. As the OCS, ZVDD and EI shapers are used for performance comparisons, their formulations are also described.

3.1. Output-based command shaper (OCS)

The OCS was previously designed based upon a measured output of a reference model and the actual 3D crane system, at a particular payload cable length [26]. The parameters of the OCS were calculated offline based on the output data and they were constants. Therefore, during a payload hoisting and in the presence of wind disturbance, where the system's parameters change, the OCS parameters could not adapt to these changes. Fig. 3 shows the block diagram of the OCS, where $G_F(s), G_a(s)$ and $G_r(s)$ represent the transfer functions of the OCS shaper, actual crane and reference model respectively. In this section, formulations used to calculate the OCS parameters are briefly described. Detail formulations can be obtained in [26].

The design of OCS consists of the following steps:

(a) To identify the order of the linear model of the system.
(b) To select a reference model of the same order with two goals: (1) the reference model should produce a low sway with a reference step input, and (2) the reference model should also be chosen to achieve a desired response time.

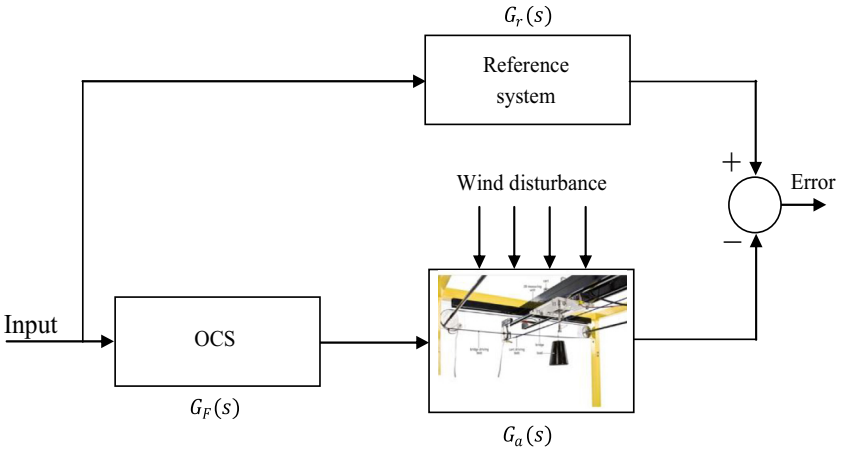

Fig. 3. A block diagram of the OCS.

(c) To design the OCS based on the system's model and the selected reference model. The OCS will be designed such that its zeros will cancel the poles of the system and replace the system poles with that of the reference model.

By using an identification method as described in [26], a linear model in a transfer function that relates the trolley position of the crane system to the input torque at a cable length of 0.47 m was obtained as

$$G_a(s) = \frac{0.7601s + 67.79}{s^4 + 10.03s^3 + 23.72s^2 + 213.5s} \tag{6}$$

Similarly, the reference model was chosen as

$$G_r(s) = \frac{16}{s^4 + 8s^3 + 24s^2 + 32s + 16} \tag{7}$$

Therefore, the OCS shaper $G_F(s)$ is derived to ensure $G_a(s)G_F(s) = G_r(s)$ as

$$G_F(s) = \frac{a_4s^4 + a_3s^3 + \cdots + a_1s + a_0}{s^4 + 8s^3 + 24s^2 + 32s + 16} \tag{8}$$

The design objective is to have the zeros of $G_F(s)$ to cancel the poles of $G_a(s)$, where the parameters $\{a_4, a_3, a_2, a_1, a_0\}$ are the design variables. By following the design steps, the OCS for the crane system can be obtained as

$$G_F(s) = \frac{0.3882s^4 + 2.4672s^3 + 8.0883s^2 + 50.3816s}{s^4 + 8s^3 + 24s^2 + 32s + 16} \tag{9}$$

The OCS shaper in Eq. (9) was shown to provide a significant payload sway reduction [26]. However, it was found that the OCS could not handle external disturbances and there is a need to improve its performance for the payload hoisting operation.

3.2. Online adaptive output-based command shaping (AOCS)

In this work, a new online adaptive algorithm based on the work in [35] is proposed. The algorithm is derived such that the parameters of AOCS can be updated online to ensure that the crane system dynamic follows the selected reference model for all conditions. In addition, this is to ensure a considerable reduction in the transient sway due to payload force of inertia and acceleration during starting and stopping phases of the crane motion. Fig. 4 shows the block diagram of the proposed adaptive command shaping, where y and y_r are the actual system and reference system outputs respectively. The trolley position is considered as the output of the system.

The adaptive formulation can be derived based on the transfer function of the OCS shaper in Eq. (8) as

$$y_k = f_k G_a(s) r, \quad k = 0, 1, 2, 3, 4.$$

where

$$f_0 = \frac{1}{s^4 + 8s^3 + 24s^2 + 32s + 16}; \; f_1 = \frac{s}{s^4 + 8s^3 + 24s^2 + 32s + 16}$$

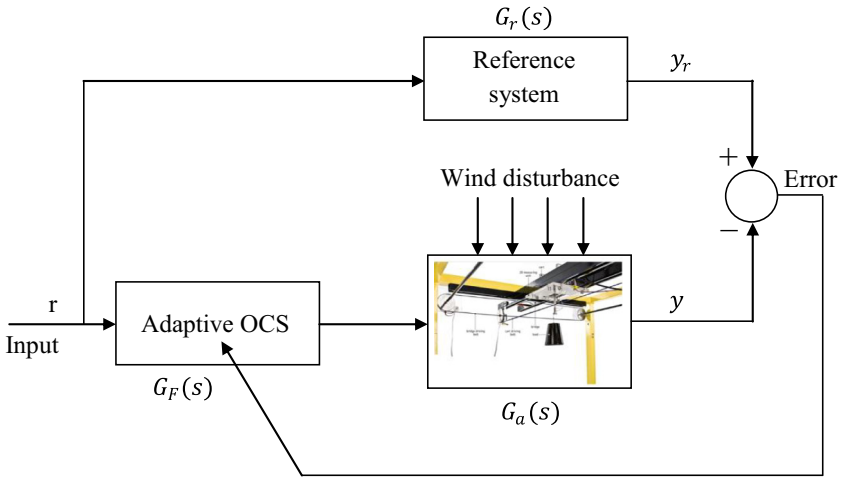

Fig. 4. A block diagram for the implementation of an adaptive command shaper.

$$f_2 = \frac{s^2}{s^4 + 8s^3 + 24s^2 + 32s + 16};\ f_3 = \frac{s^3}{s^4 + 8s^3 + 24s^2 + 32s + 16}$$

$$f_4 = \frac{s^4}{s^4 + 8s^3 + 24s^2 + 32s + 16}$$

and

$$y_r = G_r(s)r$$

Hence, the output signal of $G_F(s)G_a(s)r$ can be described as

$$y(t) = \sum_{i=0}^{k} a_k y_k(t) \tag{10}$$

where a_k are the adaptive parameters and $y_k(t)$ are the output data. A cost function is defined in order to estimate the difference between the outputs of the reference model and the actual crane system as

$$E = \int_0^t \left(\sum_{i=0}^{k} a_k y_k(t) - y_r(t) \right)^2 dt \tag{11}$$

The minimum value of E can be obtained by solving $\frac{\partial E}{\partial a_k} = 0$ as

$$\frac{\partial E}{\partial a_k} = \int_0^t y_k(t) \sum_{i=0}^{k} a_k y_k(t) - y_r(t) dt = 0 \tag{12}$$

As the objective is to achieve zero error between the actual and reference system then, $y(t) - y_r(t) = 0$, and Eq. (11) can be obtained as

$$y(t) = y_r(t) = \sum_{i=0}^{4} a_k y_k(t) \tag{13}$$

Thus, Eq. (13) can be written as

$$y_r(t) = a_4 y_4(t) + a_3 y_3(t) + a_2 y_2(t) + a_1 y_1(t) + a_0 y_0(t) \tag{14}$$

The shaper parameters $\{a_4, a_3, a_2, a_1, a_0\}$ in Eq. (14) can be updated based on the system dynamics by solving through adaptive algorithms. The right hand side of Eq. (14) can be represented as a linear relationship between the regression and estimation vectors as

$$\hat{y}(i) = e_v[n] r_v[i]^T \tag{15}$$

where $e_v[n] = [a_4 a_3 a_2 a_1 a_0]$ is the estimation vector for n number of estimated parameters, and $r_v(i) = [y_4(i) y_3(i) y_2(i) y_1(i) y_0(i)]^T$ is the regression vector for i number of iterations. Thus, the adaptive algorithm can be derived using the following least-square criterion of the error, E between the estimated and actual parameters as

$$E[e_v(n)] = \sum_{i=1}^{n} p^{n-i} (\hat{y}(i) - e_v(n) r_v(i)^T)^2 + q |e_v(n) - e_v(n-1)|^2 \tag{16}$$

where p and q are the forgetting and the weighting vectors respectively, which determine the different between the current and the previous parameter estimations. The best estimate values with a minimum error can be obtained by solving the derivative of the error with respect to the estimation vector as

$$\frac{dE}{de_v(n)} = -2 \sum_{i-1}^{n} p^{n-i} (\hat{y}(i) - e_v(n) r_v(i)^T) r_v(i) + 2q |e_v(n) - e_v(n-1)| = 0 \tag{17}$$

By collecting the similar terms in Eq. (16), the estimation vector can be obtained as

$$e_v(n) = \left(p^{n-i} \sum_{i=1}^{n} (r_v(i) r_v(i)^T) + qI \right)^{-1} \left(p^{n-i} \sum_{i=1}^{n} (\hat{y}(i) r_v(i)) + q e_v(n-1) \right) \tag{18}$$

where I is an identity matrix. Let $\Re(n)$ be the first term of the right side of Eq. (18), i.e. batch least-square form, the recursive least-square form can be deduced by taking the inverse of $\Re(n)$ as

$$\Re(n)^{-1} = p \Re(n-1)^{-1} + r_v(n) r_v(n)^T + q(1-p)I \tag{19}$$

With $\Psi(n) = \Re(n)^{-1}$, Eq. (19) can be rewritten as

$$\Psi(n) = p\Psi(n-1) + r_v(n)r_v(n)^T + q(1-p)I \tag{20}$$

and the batch form can be obtained as

$$\Psi(n)e_v(n) = (p^{n-i}\sum_{i=1}^{n}(\hat{y}(i)r_v(i)) + qe_v(n-1)) \tag{21}$$

Eq. (21) can also be shown in a recursive least-square form as

$$\Psi(n)e_v(n) = \hat{y}(n)r_v(n) + p(\Psi(n-1)e_v(n-1)) - qpe_v(n-2) + qe_v(n-1) \tag{22}$$

Similarly, Eq. (20) can be obtained as

$$p\Psi(n-1) = \Psi(n) - r_v(n)r_v(n)^T - q(1-p)I \tag{23}$$

Substituting Eq. (23) into Eq. (22) and simplifying yields

$$e_v(n) = e_v[n-1] + \Psi[n]^{-1}r_v[n](\hat{y}(n) - r_v^T[n]e_v[n-1]) + qp\Psi[n]^{-1}(e_v[n-1] - e_v[n-2]) \tag{24}$$

As $\Psi(n) = \Re(n)^{-1}$, Eq. (24) can be written as

$$e_v[n] = e_v[n-1] + \Re[n]r_v[n](\hat{y}(n) - r_v^T[n]e_v[n-1]) + qp\Re[n](e_v[n-1] - e_v[n-2]) \tag{25}$$

Eqs. (20) and (25) are the adaptive algorithm equations with initial condition as $\Re^{-1}[0] = qI$ and the constant terms p and q are chosen as $0 < p < 1$ and $q > 0$.

3.3. Input shaping

In this work, ZVDD and EI shapers were designed and implemented on the overhead crane for performance comparisons with the proposed AOCS. Both the ZVDD and EI are input shapers designed based on the impulse sequence using a natural frequency and damping ratio of a system. Both are considered as robust input shapers and to enhance their performances and robustness for handling payload hoisting and wind disturbance, they were designed based on the frequency and damping ratio of the system at the ATL of the hoisting cable. In this work, as the overhead crane operates in the hoisting range of 0.22–0.72 m, the average hoisting length is 0.47 m and this corresponds to the natural frequency and damping ratio of 4.57 rad/s and 0.008 respectively. The ZVDD and EI shapers designed based on the ATL are referred as ATL-ZVDD and ATL-EI respectively in this work. The designs of the two robust shapers are briefly described.

3.3.1. Zero vibration derivative-derivative shaper (ATL-ZVDD)

Any oscillatory system can be modelled as a superposition of second order systems, each with a transfer function as

$$G(s) = \frac{\omega_n^2}{s^2 + 2\zeta\omega_n s + \omega_n^2} \tag{26}$$

where ω_n is the natural frequency and ζ is the damping ratio of the system at the average travel hoisting length. In a time domain, the response of the system can be expressed as

$$y(t) = \frac{A\omega_n}{\sqrt{(1-\zeta^2)}}e^{-\zeta\omega_n(t-t_0)}\sin\left(\omega_n(t-t_0)\sqrt{(1-\zeta^2)}\right) \tag{27}$$

where A and t_0 are the amplitude and time instant of the impulse respectively. By superposition, the response to a sequence of impulses after the last impulse can be obtained as

$$y(t) = \sum_{k=1}^{N}\left[\frac{A_k\omega_n}{\sqrt{(1-\zeta^2)}}e^{-\zeta\omega_n(t-t_k)}\right]\sin\left(\omega_n(t-t_k)\sqrt{(1-\zeta^2)}\right) \tag{28}$$

Residual single mode vibration amplitude of the impulse response can be obtained at the time of the last impulse t_k as

$$V(\omega_n,\zeta) = e^{-\zeta\omega_n t_k}\sqrt{R_1^2 + R_2^2} \tag{29}$$

where

$$R_1 = \sum_{k=1}^{N}A_k e^{\zeta\omega_n t_k}\sin\left(\omega_n t_k\sqrt{(1-\zeta^2)}\right)$$

and

$$R_2 = \sum_{k=1}^{N} A_k e^{\zeta\omega_n t_k} \cos\left(\omega_n t_k \sqrt{(1-\zeta^2)}\right)$$

Solving Eq. (29) for $V(\omega_n, \zeta) = 0$, yields a two impulse sequence input shaper known as zero vibration (ZV). It was shown that a more robust shaper can be obtained by solving derivatives of the residual vibration amplitude. Fig. 5 shows the ATL-ZVDD shaping process with a four-impulse sequence. In order to avoid a response delay, $t_1 = 0$ was chosen. The ATL-ZVDD design parameters were deduced as [36]

$$\begin{bmatrix} A_k \\ t_k \end{bmatrix} = \begin{bmatrix} \frac{1}{(1+K)^3} & \frac{3K}{(1+K)^3} & \frac{3K^2}{(1+K)^3} & \frac{K^3}{(1+K)^3} \\ 0 & \tau_d & 2\tau_d & 3\tau_d \end{bmatrix} \tag{30}$$

where

$$\tau_d = \frac{\pi}{\omega_n \sqrt{(1-\zeta^2)}}$$

and

$$K = e^{\frac{-\pi\zeta}{\sqrt{(1-\zeta^2)}}}$$

3.3.2. Extra insensitive shaper (ATL-EI)

The design of ATL-EI shaper is basically similar to the design of ZV and ZVDD shapers. However, in the EI input shaping, the residual vibration, $V(\omega_n, \zeta)$ is set to a nonzero value. By relaxing the zero vibration constrains to a certain value greater than zero, the robustness of the input shaping can be increased. The same values of ω_n and ζ at the average travel hoisting length were used for the design of ATL-EI. The formulation of ATL-EI shaper in this work is as derived in [37] as

$$V(\omega_n, \zeta) = V_{tol}(> 0) \tag{31}$$

where $V_{tol}(> 0)$ is a non-zero value of the residual vibrations. The approximate numerical solution of the ATL-EI shaper for underdamped systems was obtained by using optimization software with the assumption that the system's damping ratio is within the range of $0 < \zeta \leqslant 0.3$ and the residual vibration is in the range of $0 < V_{tol} \leqslant 0.15$ [37]. The optimized solution for underdamped systems is given as

$$A_1 = 0.24968 + 0.24962V_{tol} + 0.80008\zeta + 1.23328V_{tol}\zeta + 0.49599\zeta^2 + 3.17316V_{tol}\zeta^2 \tag{32}$$

$$A_2 = 1 - (A_1 + A_3) \tag{33}$$

$$A_3 = 0.25149 + 0.21474V_{tol} - 0.83249\zeta + 1.41498V_{tol}\zeta + 0.85181\zeta^2 - 4.90094V_{tol}\zeta^2 \tag{34}$$

$$t_1 = 0 \tag{35}$$

$$t_2 = (0.49990 + 0.46159V_{tol}\zeta + 4.26169V_{tol}\zeta^2 + 1.75601V_{tol}\zeta^3 + 8.57843V_{tol}^2\zeta - 108.644V_{tol}^2\zeta^2 + 336.989V_{tol}^2\zeta^3)T_d \tag{36}$$

$$t_3 = T_d = 2\pi \Big/ \left(\hat{\omega}\sqrt{1-\zeta^2}\right) \tag{37}$$

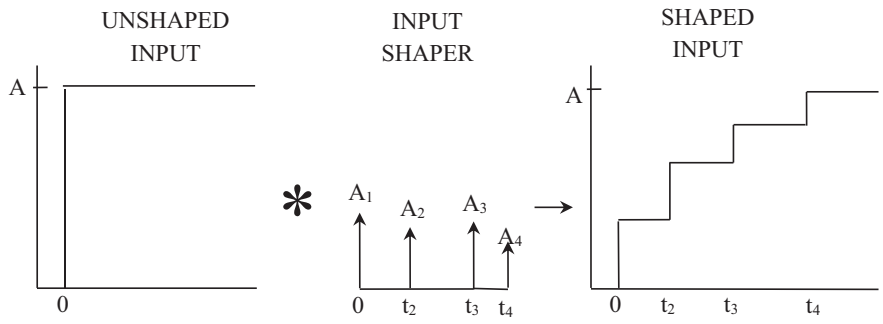

Fig. 5. ATL-ZVDD shaping process.

Table 2
Parameters of ATL-ZVDD and ATL-EI shapers.

Shapers	Magnitudes				Time locations (s)			
	A_1	A_2	A_3	A_4	t_1	t_2	t_3	t_4
ATL-ZVDD	0.1286	0.3785	0.3714	0.1215	0	0.8423	1.6845	2.5268
ATL-EI	0.2674	0.4750	0.2577	–	0	0.6938	1.3870	–

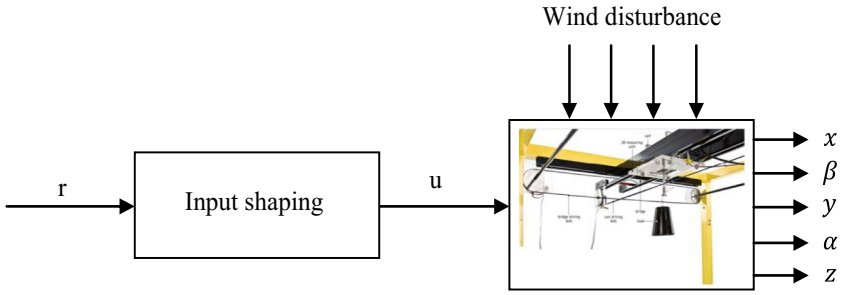

Fig. 6. A block diagram for the implementation of ZVDD and EI shapers.

where $\hat{\omega}$ is a modelled frequency with a modelling error such that $\hat{\omega} \neq \omega_n$. It is assumed that $\omega_n = \hat{\omega} + \eta$ where η is a constant representing the value of the modelling error.

Considering the crane's parameters with the average travel hoisting length of 0.47 m, and solving Eq. (30) and Eqs. (32)–(37), the parameters of the ATL-ZVDD and ATL-EI shapers were obtained as presented in Table 2.

4. Implementation and experimental results

This section describes the real-time implementations of the AOCS, OCS, ATL-ZVDD and ATL-EI shapers on the laboratory overhead crane as shown in Fig. 1. Control of simultaneous motions of the trolley and payload hoisting in the presence of wind disturbance force were investigated using the command shapers. Due to the limitation of the crane, a payload hoisting of between 0.22 m and 0.72 m was considered which corresponded to decrements in the system's natural frequency and damping ratio by 42% and 54%, respectively. The performances of the control schemes were tested based on the following two cases:

- Case I: Simultaneous motion of the trolley and payload hoisting with payloads of 1 kg and 0.5 kg.
- Case II: Simultaneous motion of the trolley and payload hoisting in the presence of wind disturbance of magnitude 0.3 N with payloads of 1 kg and 0.5 kg.

In this work, a condition where the wind disturbance is in the direction of the trolley motion is considered. In this condition, the wind has significant effects which amplify the magnitude of the sway. Two different payloads of 1 kg and 0.5 kg were considered. For a valid comparison, they are of the same size and shape but made up of different materials. It is expected that the wind disturbance gives higher sway to the lighter payload. The command and input shapers were implemented on the laboratory crane and the payload sway responses were monitored for 20 s.

The performance of the AOCS technique when compared with the OCS, ATL-ZVDD and ATL-EI shapers was assessed in terms of the level of sway reductions, robustness to the changes in the system parameters (cable lengths and payloads) and to the wind disturbance. As the objective is to obtain a zero sway, a mean square error (MSE) can be used as a performance index, in which a small value of MSE indicates a low overall sway response. Furthermore, the level of maximum transient sway (MTS) was also measured and compared, where a low value of MTS is desirable. Figs. 3 and 4 show the block diagrams of the OCS and AOCS respectively. On the other hand, Fig. 6 shows a block diagram for a payload sway motion control of the crane system using the ATL-ZVDD and ATL-EI shapers. In this work, a pulse signal with amplitude of 0.5 N and a width of 3 s, as shown in Fig. 7, is used as the input signal where a suitable system response for the performance investigations can be obtained.

4.1. System response without an input/command shaper

Initially, to study the effects of the payload hoisting and wind disturbance, payload sway responses of the overhead crane without an input/command shaper for payloads of 0.5 kg and 1 kg were obtained and analysed. Fig. 8 shows the sway responses of the overhead crane without the input/command shaping. For the case with hoisting only, it was noted that

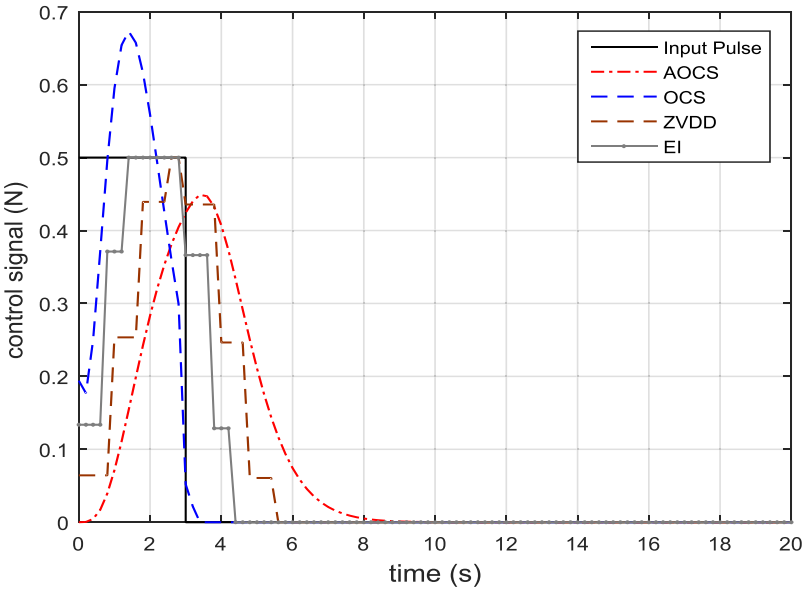

Fig. 7. Unshaped and shaped input signals.

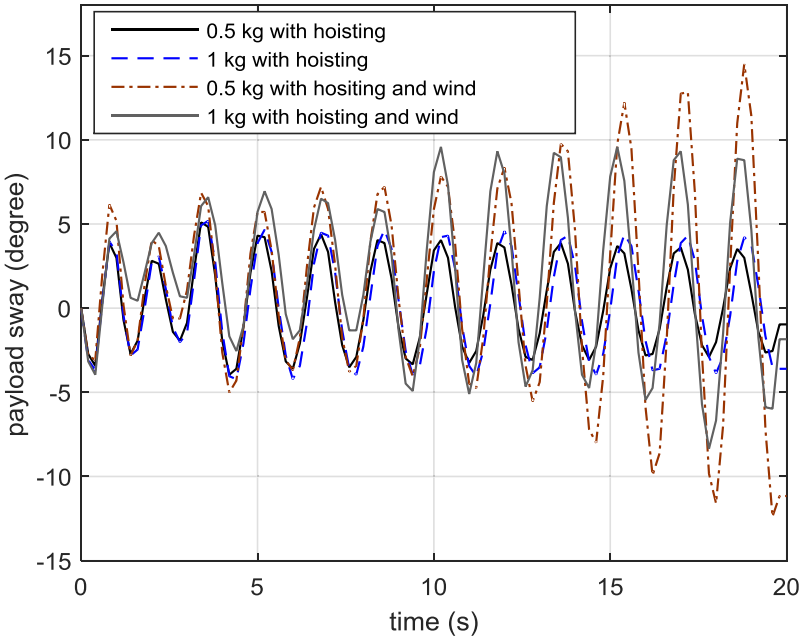

Fig. 8. Payload sways of the crane without input/command shaping.

the sways are within ±4 degrees and payload mass variations have small effects on the sway. On the other hand, for the case with payload hoisting and wind disturbance, higher payload sways as compared to the previous case were noted, especially for the residual sways that increase with time. As expected, the wind affected more on the lighter payload, where a significant residual sway was demonstrated. The MSE and MTS values for the two cases are given in Table 3.

A further analysis on the results shows that the wind has significantly increased the payload sways. For both payloads, the MSE and MTS values increased more than 71% and 47% respectively. Furthermore, with the wind disturbance, the MSE and MTS values for the lighter payload increased by 56% and 51% respectively, when compared with the payload of 1 kg. As the effects of both hoisting and wind are significant, it is important to develop a control strategy to reduce the transient and residual sways and to provide a uniform performance under all conditions.

Table 3
MSE and MTS values for payload sway responses without input/command shaping.

Values	Hoisting		Hoisting and wind	
	0.5 kg payload	1.0 kg payload	0.5 kg payload	1.0 kg payload
MSE	9.1592	6.8274	37.3073	23.9029
MTS	5.1856	5.0977	14.5021	9.5802

MSE: Mean square error; MTS: Maximum transient sway.

4.2. Results with input/command shapers

By using the designed AOCS, OCS, ATL-ZVDD, and ATL-EI, shaped input signals as shown in Fig. 7 were obtained and applied into the crane system. Figs. 9 and 10 show the sway responses of the AOCS, OCS, ATL-ZVDD, and ATL-EI shapers for Case I with payloads of 1 kg and 0.5 kg respectively. It can be observed that all the shapers were able to reduce the overall

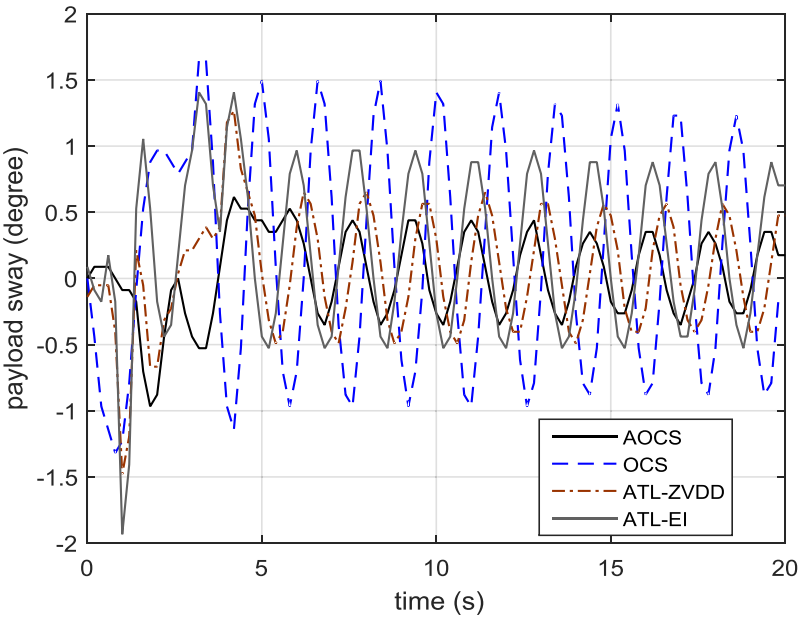

Fig. 9. Payload sways of the crane with hoisting (payload of 1 kg).

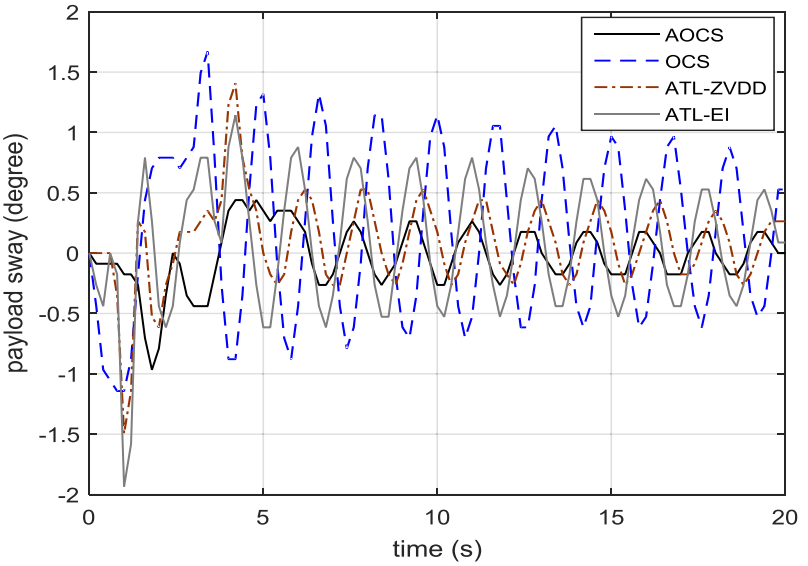

Fig. 10. Payload sways of the crane with hoisting (payload of 0.5 kg).

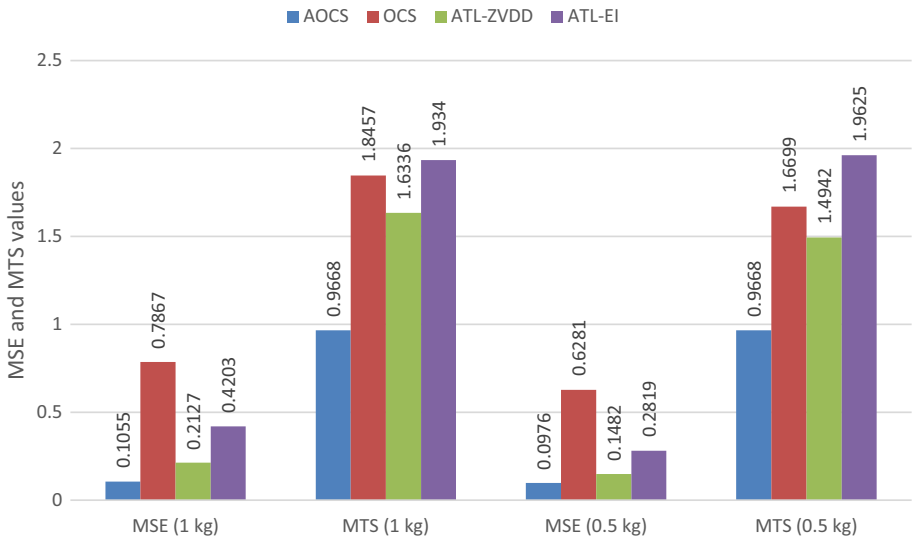

Fig. 11. MSE and MTS values of the payload sways with hoisting.

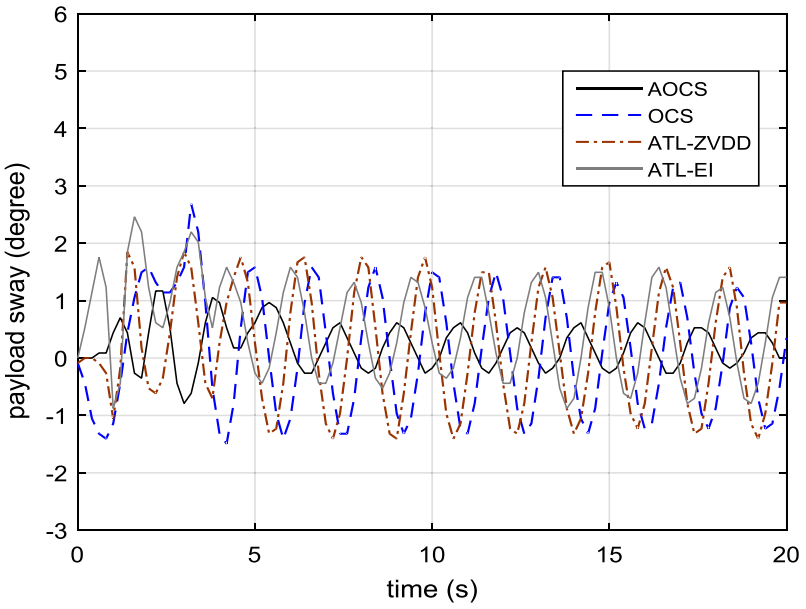

Fig. 12. Payload sways of the crane with hoisting and wind (payload of 1 kg).

sways as compared to the unshaped response (Fig. 8), with the highest sway was noted about ±1.5 degrees. The MSE and MTS values achieved with the shapers are shown in Fig. 11. For both payloads, the shapers reduced the overall sway (MSE) and MTS values at least by 88% and 62% respectively when compared to the unshaped sway response. On the other hand, the proposed AOCS shaper was found to be superior when compared to the other approaches, where the AOCS resulted in the lowest MSE and MTS values. The proposed adaptive input shaping was capable of handling the payload hoisting with residual sways of ±0.4 and ±0.2 degrees for payloads of 1 kg and 0.5 kg respectively.

For Case II, experiments involving the overhead crane with hoisting in the presence of wind disturbance were conducted. Robustness performance of the controllers will be more apparent as the dynamic behaviour of the crane changes significantly as demonstrated in Fig. 8. Figs. 12 and 13 show payload sway responses using all the controllers with payloads of 1 kg and 0.5 kg respectively. It was clearly shown that the AOCS shaper outperformed all the other controllers especially for the case with a payload of 0.5 kg. The overall sway (MSE value) and the MTS value achieved using all the controllers are shown in Fig. 14. It was also observed that the ATL-ZVDD shaper provided a better performance as compared to the

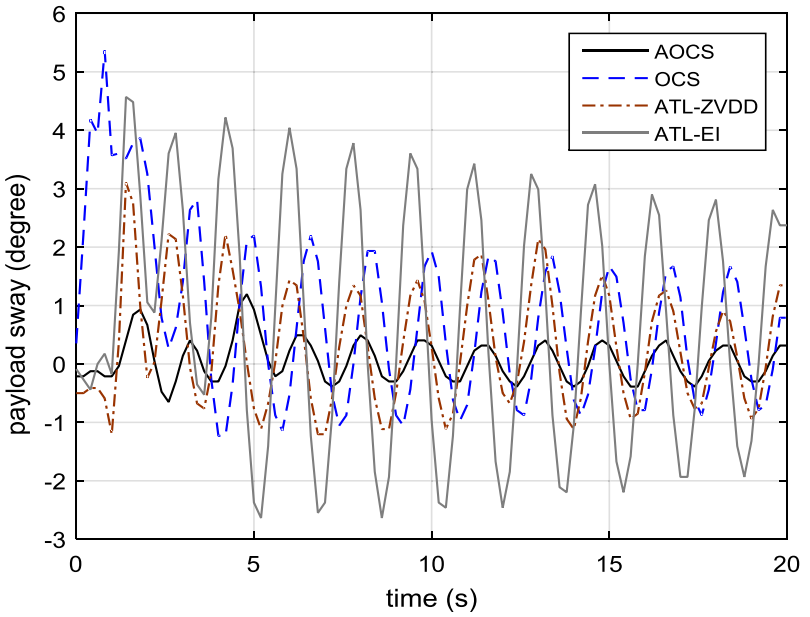

Fig. 13. Payload sways of the crane with hoisting and wind (payload of 0.5 kg).

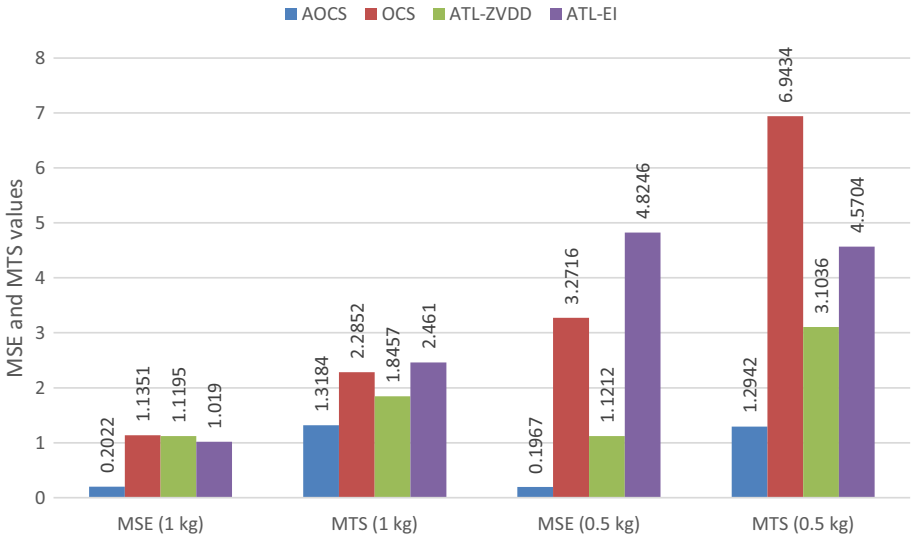

Fig. 14. MSE and MTS values of the payload sways with hoisting and wind disturbance.

OCS and ATL-EI shapers. Nevertheless, the AOCS shaper has the lowest sway and has reduced the MSE values obtained using the ATL-ZVDD shaper by 82% and 83% for payloads of 1 kg and 0.5 kg respectively. On the other hand, reductions of 29% and 58% in the MTS values were achieved with the AOCS shapers for payloads of 1 kg and 0.5 kg respectively when compared to the ATL-ZVDD.

In addition, the proposed AOCS was shown to be robust and was capable to adapt to the changes in the system dynamics. This resulted in a uniform performance in the payload sway of the laboratory crane with hoisting and wind disturbance, and with different payloads. Although the wind resulted in a higher sway for the lighter payload, the AOCS was able to handle and provided a similar sway response as the case with another payload. Fig. 15 illustrates the changes in the AOCS parameters to adapt to the system changes. The parameter a_0 changes between 16 and 17.2. To further demonstrate the performance of the controllers, Figs. 16 and 17 show the values of MSE and MTS obtained using the controllers with payload variations for Case II. It was found that with the AOCS, besides the lowest MSE and MTS values when compared to the other

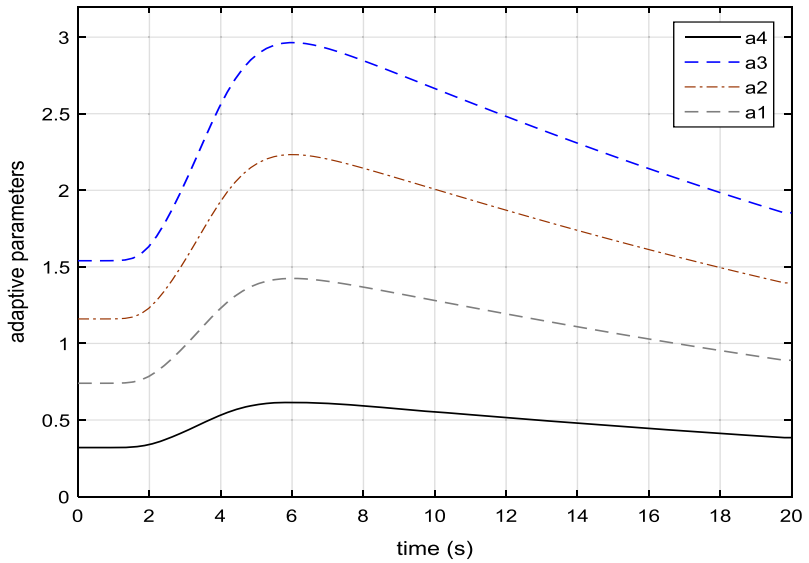

Fig. 15. Parameters of the AOCS with hoisting and wind disturbance.

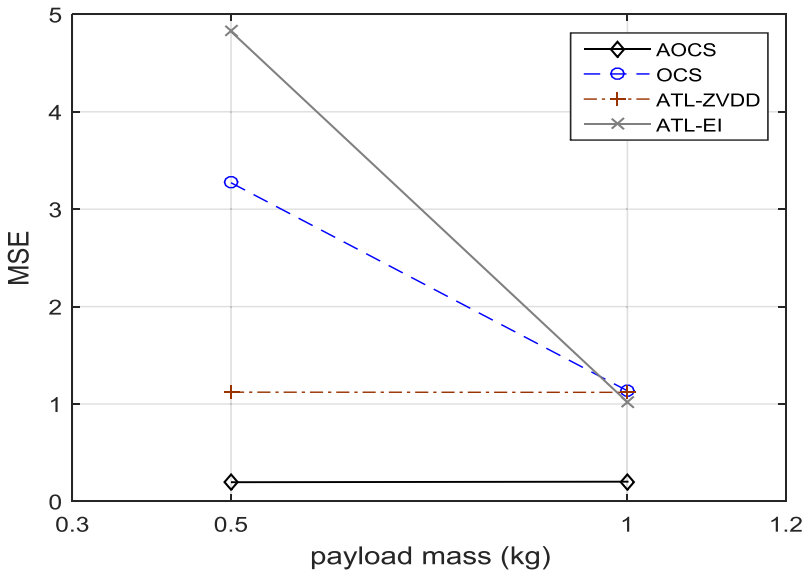

Fig. 16. MSE values of the payload sways of the crane with different payloads.

controllers, the performance is almost identical for both payloads. This is a clear advantage for control of unknown payloads with an external disturbance. In contrast, with other approaches, significant differences were noted for both MSE and MTS values.

5. Conclusion

A new online adaptive output-based command shaping was designed for payload sway reductions of a 3D overhead crane with hoisting and in the presence of wind disturbance. Different payload weights were also investigated as the wind has a considerable effect on a lighter payload. For performance comparisons, the OCS, and two robust input shapers namely ATL-ZVDD and ATL-EI shapers were also designed and implemented. Experimental results have shown that the

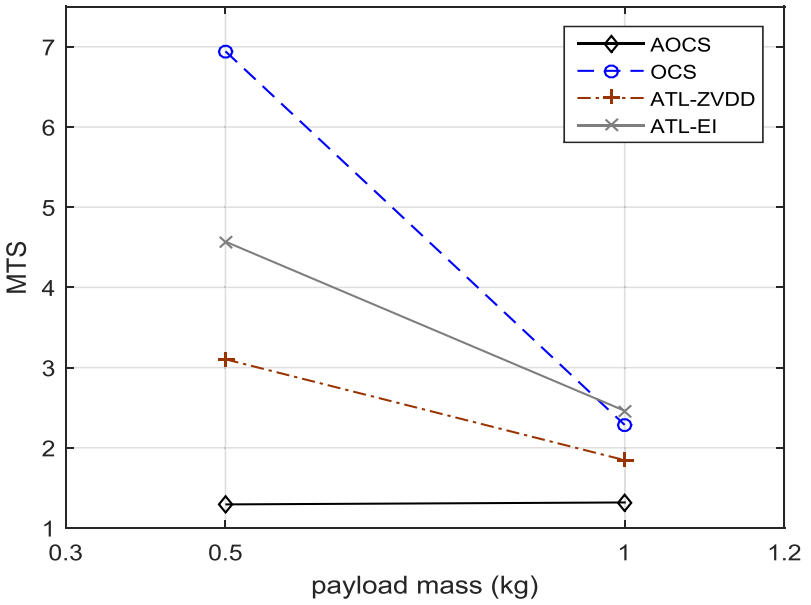

Fig. 17. MTS values of the payload sways of the crane with different payloads.

AOCS shaper provides the highest reductions in the overall sway, transient sway and residual sway, and is able to handle the effects of hoisting and wind disturbance. With different payloads, a uniform performance is achieved with the proposed AOCS.

References

[1] N.B. Almutairi, M. Zribi, Sliding mode control of a three-dimensional overhead crane, J. Vib. Control 15 (2009) 1679–1730.
[2] Z.N. Masoud, M.F. Daqaq, A graphical approach to input-shaping control design for container cranes with hoist, IEEE Trans. Control Syst. Technol. 14 (2006) 1070–1077.
[3] Y. Jisup, S. Nation, W. Singhose, J.E. Vaughan, Control of crane payloads that bounce during hoisting, IEEE Trans. Control Syst. Technol. 22 (2014) 1233–1238.
[4] H.M. Omar, A.H. Nayfeh, Gantry cranes gain scheduling feedback control with friction compensation, J. Sound Vib. 28 (2005) 1–20.
[5] J. Smoczek, Fuzzy crane control with sensorless payload deflection feedback for vibration reduction, Mech. Syst. Signal Process. 46 (2014) 70–81.
[6] L. Ramli, Z. Mohamed, A.M. Abdullahi, H.I. Jaafar, I.M. Lazim, Control strategies for crane systems: a comprehensive review, Mech. Syst. Signal Process. 95 (2017) 1–23.
[7] S. Garrido, M. Abderrahim, A. Giménez, R. Diez, C. Balaguer, Anti-swinging input shaping control of an automatic construction crane, IEEE Trans. Autom. Sci. Eng. 5 (2008) 549–557.
[8] M. Zhang, X. Ma, X. Rong, X. Tian, Y. Li, Error tracking control for underactuated overhead cranes against arbitrary initial payload swing angles, Mech. Syst. Signal Process. 84 (2017) 268–285.
[9] M. Zhang, X. Ma, X. Rong, X. Tian, Y. Li, Adaptive tracking control for double-pendulum overhead cranes subject to tracking error limitation, parametric uncertainties and external disturbances, Mech. Syst. Signal Process. 76–77 (2016) 15–32.
[10] Z. Zhang, Y. Wu, J. Huang, Differential-flatness-based finite-time antiswing control underactuated crane system, Nonlinear Dyn. 87 (2017) 1749–1761.
[11] N. Sun, Y. Fang, H. Chen, B. Lu, Amplitude-saturated nonlinear output feedback antiswing control for underactuated cranes with double-pendulum cargo dynamics, IEEE Trans. Industr. Electron. 64 (2017) 2135–2146.
[12] G.N. Glossiotis, I. Antoniadis, Payload sway suppression in rotary cranes by digital filtering of the commanded inputs, Proc. Inst. Mech. Eng., J. Multi-Body Dyn. 217 (2003) 99–109.
[13] G.N. Glossiotis, I. Antoniadis, Digital filter based motion command preconditioning of time varying suspended loads in boom cranes for sway suppression, J. Vib. Control 13 (2007) 617–656.
[14] X. Xie, J. Huang, Z. Liang, Vibration reduction for flexible systems by command smoothing, Mech. Syst. Signal Process. 39 (2013) 461–470.
[15] J. Huang, Z. Liang, Q. Zang, Dynamics and swing control of double-pendulum bridge cranes with distributed-mass beams, Mech. Syst. Signal Process. 54 (2015) 357–366.
[16] J. Huang, X. Xie, Z. Liang, Control of bridge cranes with distributed-mass payload dynamics, IEEE/ASME Trans. Mechatron. 20 (2015) 481–486.
[17] R. Tang, J. Huang, Control of bridge cranes with distributed-mass payloads under windy conditions, Mech. Syst. Signal Process. 72–73 (2016) 409–419.
[18] N. Singer, W. Seering, Pre-shaping command inputs to reduce system vibration, ASME J. Dyn. Syst., Measur., Control. 112 (1990) 76–82.
[19] S.S. Gurleyuk, O. Bahadir, Y. Turkkan, H. Usenti, Improved three-step input shaping control of crane system, WSEAS Trans. Syst. 6 (2008) 652–661.
[20] K.T. Hong, C.D. Huh, K.S. Hong, Command shaping control for limiting the transient sway angle of crane systems, Int. J. Control Autom. Syst. 1 (2003) 43–53.
[21] M.A. Ahmad, R.R. Ismail, M.S. Ramli, R.E. Samin, M.A. Zawawi, Robust input shaping for anti-sway control of rotary crane, in: The Proceedings of IEEE Region 10 Conference (TENCON), 2009, pp. 1–5.
[22] K.L. Sorensen, K. Hekman, W.E. Singhose, Finite-state input shaping, IEEE Trans. Control Syst. Technol. 18 (2010) 664–672.
[23] L. Yan-yang, W. Xiong, Input shaping anti-swing controller design and robustness analysis for crane system, in: Proceedings of the 13th Chinese Control Conference, Hefei, China, 2012, pp. 4502–4506.
[24] M.J. Maghsoudi, Z. Mohamed, M.O. Tokhi, A.R. Husain, M.S.Z. Abidin, Control of a gantry crane using input-shaping schemes with distributed delay, Trans. Inst. Measur. Control 39 (2017) 361–370.

[25] M.J. Maghsoudi, Z. Mohamed, S. Sudin, S. Buyamin, H.I. Jaafar, S.M. Ahmad, An improved input shaping design for an efficient sway control of a nonlinear 3D overhead crane with friction, Mech. Syst. Signal Process. 92 (2017) 364–378.
[26] A.M. Abdullahi, Z. Mohamed, M.S. Zainal Abidin, S. Buyamin, A.A. Bature, Output-based command shaping technique for an effective payload sway control of a 3D crane with hoisting, Trans. Inst. Measur. Control, doi:http://dx.doi.org/10.1177/0142331216640871 (in press).
[27] J. Stergiopoulos, A. Tzes, An adaptive input shaping technique for the suppression of payload swing in three-dimensional overhead cranes with hoisting mechanism, in: IEEE International Conference on Emerging Technology, Factory Automation, Patras, Greece, 2007, pp. 565–568.
[28] J. Stergiopoulos, G. Konstantopoulos, A. Tzes, Experimental verification of an adaptive input shaping scheme for hoisting cranes, in: Proceedings of IEEE Mediterranean Conference on Control and Automation, 2009, pp. 730–735.
[29] M. Gniadek, Robustness analysis of super-robust and adaptive algorithm of input shaping, Poznan Univ. Technol. Acad. J. 1 (2015) 195–202.
[30] J.M. Veciana, S. Cardona, P. Català, Modified adaptive input shaping for maneuvering cranes using a feedback MEM gyroscope with null drift, Int. J. Precision Eng. Manuf. 16 (2015) 1911–1917.
[31] W. Singhose, L. Porter, M. Kenison, E. Kriikku, Effects of hoisting on the input shaping control of gantry cranes, Control Eng. Practice 8 (2000) 1159–1165.
[32] J. Huang, E. Maleki, W. Singhose, Dynamics and swing control of mobile boom cranes subject to wind disturbances, IET Control Theory Appl. 7 (2013) 1187–1195.
[33] J. Tomczyk, J. Cink, A. Kosucki, Dynamics of an overhead crane under a wind disturbance condition, Autom. Constr. 4 (2014) 100–111.
[34] J. Han, Z. Zhu, Y. He, J. Qi, A novel input shaping method based on system output, J. Sound Vib. 335 (2015) 338–349.
[35] M. Bodson, An adaptive algorithm for the tuning of two input shaping methods, Automatica 34 (1998) 771–776.
[36] W.E. Singhose, N.C. Singer, W.P. Seering, Comparison of command shaping methods for reducing residual vibration, in: Proceedings of European Control Conference, Rome, Italy, 1995, pp. 1126–1131.
[37] K. Chul-Goo, H. Manh-Tuan, Partially analytical extra-insensitive shaper for a lightly damped flexible arm, in: Proceedings of IEEE international Conference on Intelligent Robots and Systems, Chicago, USA, 2014, pp. 2401–2406.